Egyptian Journal of Petroleum (2016) **25**, 269–279

HOSTED BY

Egyptian Petroleum Research Institute

**Egyptian Journal of Petroleum**

www.elsevier.com/locate/egyjp
www.sciencedirect.com

FULL LENGTH ARTICLE

# Copper nanoparticles supported onto montmorillonite clays as efficient catalyst for methylene blue dye degradation

**M.A. Mekewi [a], A.S. Darwish [a], M.S. Amin [a], Gh. Eshaq [b], H.A. Bourazan [c,*]**

[a] *Department of Chemistry, Faculty of Science, Ain Shams University, Cairo, Egypt*
[b] *Department of Petrochemicals, Egyptian Petroleum Research Institute, Nasr City, Cairo 11727, Egypt*
[c] *Department of chemistry, Faculty of Science, Aleppo University, Syria*

Received 25 May 2015; revised 19 June 2015; accepted 22 June 2015
Available online 21 January 2016

**KEYWORDS**

Nano Cu/Clay;
MB dye;
Kinetic model

**Abstract** The paper describes the production of copper nanoparticles through the reduction of copper chloride ($CuCl_2{\cdot}2H_2O$) by hydrazine in the aqueous cetyle trimethyl ammonium bromide (CTAB) solution. The copper nanoparticles were then supported on chemically activated Montmorillonite clay (MMT). The native and modified clays as well as synthesized Cu-nanoparticle-clay were structurally and texturally characterized by XRD, FTIR, BET, SEM and TEM in addition to the estimation of exchange capacity parameters. BET surface characterization revealed a decrease in surface area of the clay support after the incorporation of Cu nanoparticles. Cu/clay was then utilized as a catalyst for the degradation of aqueous solutions containing methylene blue (MB) over a wide pH range. Diverse kinetics models were employed to examine the degradation process revealing a better fit with pseudo-first-order model. The present study offers a novel modified clay based catalysts for the degradation of methylene blue dye contaminant from wastewater.


## 1. Introduction

Metal nanoparticles have attracted a great attention of researchers for sound applications recently especially in the field of waste water recycling. Nano metals are defined as clusters containing tens to thousands of metal atoms, and their sizes vary between one to tens of nanometers [1]. They have been considered as very attractive catalysts due to the acquired large surface area acquiring in turn higher catalytic efficiency, optical, electrical and antifungal/antibacterial applications [2–6].

The stabilizers for synthesizing nanoparticles play an important role in controlling nano size, shape as well as morphology. Various supports/stabilizers like mesoporous solid, organic ligand, polymer, carbon materials, etc. are reported [7–15]. Montmorillonite clay is one of the suitable supports where metal nanoparticles can be stabilized within the interlayer spacing or into the pores on the surface [16–19].

* Corresponding author.
E-mail address: hbourazan@hotmail.com (H.A. Bourazan).
Peer review under responsibility of Egyptian Petroleum Research Institute.

http://dx.doi.org/10.1016/j.ejpe.2015.06.011

The surface properties of MMT clay were even improved further with regard to the surface area, and porosity after having activated through acid and organic treatments making the clay appropriate for stabilizing metal nanoparticles [20,21]. Synthesis and applications of clay supported nanoparticles in catalysis is an emerging topic, when compared to the conventional homogeneous catalysts [22–24].

Supported nanoparticles play a crucial role in the degradation of dyes, which are becoming a serious environmental problem due to their inflected toxicity on humans, high chemical oxygen demand content, and biological degradation [25,26]. Among various dyes, methylene blue (MB) is difficult to degrade and is often utilized as a model dye contaminant [27].

The present study aimed to synthesize and investigate well dispersed Cu onto activated MMT clay and to examine the effectiveness of materials in immobilization and catalytic degradation of MB dye from aqueous solutions.

## 2. Experimental and methodology

### 2.1. Materials

(a) Clay mineral

Montmorillonite clay from Sadat city, Egypt was firstly washed by 0.5 M $HNO_3$ for 48 h at 60 °C prior use. The MMT clay's main characterization features were measured and found as below:

- Cation exchange capacity (CEC) = 50 meq/100 g.
- Surface area = 39.186 $m^2$/g.
- Chemical compositions: 50.29% $SiO_2$, 18.21% $Al_2O_3$, 8.38% $Fe_2O_3$, 1.72% Cao, 2.09% MgO, 3.81% $Na_2O$, 0.89% $K_2O$, 1.21% $TiO_2$, 0.19% $P_2O_5$, 0.35% $SO_3$.

(b) Chemicals

HCl, $HNO_3$, $H_2SO_4$, NaOH, NH4OH, cetyle trimethyl ammonium bromide (CTAB), copper chloride ($CuCl_2{\cdot}2H_2O$), ρ-amino benzoic acid (ρ-ABA), Hydrazine hydrate ($N_2H_4{\cdot}xH_2O$), methylene blue (MB), and Hydrogen peroxide ($H_2O_2$) were of pure analytical grades.

### 2.2. Preparation and synthesis

#### 2.2.1. Acid treated clay (AT-MMT)

The pretreated clay (100 g) was soaked in 750 ml of 2 M $H_2SO_4$ for 48 h at 70 °C. The clay was then filtered and washed with distilled water several times till neutral and finally dried at 80 °C for 24 h.

#### 2.2.2. Organo-treated clay (PA-MMT)

The ρ-amino benzoic acid was firstly prepared by dissolving 1 g in 250 ml distilled water with the addition of a few drops of HCl. Afterward, 15 g of pretreated clay was soaked in a mixture of 200 ml distilled water and 80 ml of ρ-amino benzoic acid solution for 3 days. The pH was adjusted at ~1–2 using concentrated hydrochloric acid. The resulting modified clay was then filtered and well washed with boiled distilled water several times to withdraw all adsorbed impurities and finally dried at 50 °C for 24 h.

#### 2.2.3. Cu nanoparticles immobilized onto modified clay

In a typical synthesis process, the starting solution was prepared in two conical flasks, in the first flask 0.0268 g copper chloride ($Cu\ Cl_2{\cdot}2H_2O$) was dissolved in a small amount of DI water and then 0.0286 g of CTAB was dissolved in another 10 ml DI water. After mixing both solutions, ammonia solution was gently dropped until the solution pH = 10, where the color of solution changed from light blue to dark blue without formation of any precipitate (solution-I).

In the second flask 0.05 ml hydrazine hydrate was added to 0.0286 g of CTAB already dissolved in 25 ml DI water (solution-II). Then the addition of solution-I into solution-II was performed with continuous stirring and heating till the temperature reached 80 °C. As the reaction proceeded, the solution color changed from colorless to light yellow to orange to brown and finally to red color, which confirmed the formation of metallic colloidal suspension. The reduction reaction can be expressed as:

$$2[Cu(NH_3)_2]^{2+} + N_2H_4 + 4OH^- \leftarrow 2Cu + N_2 + 4NH_4OH$$

Finally, 1 g of each modified clay samples was mixed with the metallic solution at 80 °C, the resulting paste of metal/clay nanocomposite was finally dried at 70 °C for 18 h designated as Cu/MMT.

### 2.3. Characterization techniques

#### 2.3.1. Structural characteristics of raw, modified montmorillonite samples and Cu supported modified clay nanocomposites

*2.3.1.1. XRD analysis.* Crystallinity patterns of native (Raw-MMT), acid treated (AT-MMT) and ρ-amino benzoic treated montmorillonite (PA-MMT) as well as Cu nanoparticles immobilized onto modified clay samples (Cu-AT-MMT and Cu-PA-MMT) were studied using XRD (PANalytical Xpert Pro) using Cu Kα radiation ($\lambda$ = 1.5418 Å) in the range of $2\theta$ = 5–70°.

*2.3.1.2. FT-IR spectroscopic analysis.* The chemical structural features of the native, modified and cu nanoparticle supported modified clays were assessed through FT-IR spectroscopy (FT-IR 4000 type A from Jasco Company, USA).

#### 2.3.2. Morphological studies

(a) Texture properties of raw, modified montmorillonite samples, and Cu supported modified clay nanocomposites.

The surface areas were estimated using surface area characters [28,29] (based on $N_2$ adsorption-desorption isotherms at −196 °C).

(b) Cation exchange capacity of various modified montmorillonite samples

The cation exchange capacity (CEC) of the native and tow modified clay samples were measured, in meq/100 g, using the

copper triethylenetetramine complex $[Cu(trien)_2]^{2+}$ method [30,31].

(c) Scanning electron microscopy of various modified montmorillonite samples

The crystal microstructure and the morphology of raw and modified montmorillonite samples were envisaged using scanning electron microscope (LEO 1530 FE-SEM).

(d) Transmission electron microscopy (TEM) of Cu nanoparticle modified clay nanocomposites

The shape and the size of the embedded metallic nanoparticles were inspected through high resolution transmission electron microscope (HRTEM, JEOL-2100) operating at 200 KV with resolution of 0.14 nm using a porous carbon film supported on a copper grid.

### 2.4. Catalytic activity of Cu/MMT: Degradation of MB

The degradation of methylene blue dye solution was carried out with a total volume of 50 ml at an initial concentration of $1 \times 10^{-4}$ M, and 28.91 mM of $H_2O_2$ (as an oxidant) at pH 8.0. The reaction temperature was kept at 40 ± 1 °C. Finally, 0.05 g of metal/clay nanocomposites was added to the solution initiating oxidative degradation reaction. At set intervals, 2 ml of suspension was taken from the reaction glass and analyzed spectrophotometrically using EVO300 PC, MALYZIA spectrophotometer at wavelengths ranging between 400 and 800 nm. The catalytic degradation efficiency ($E$) of MB was obtained by the following formula:

$$E = \frac{C_0 - C}{C_0} \times 100\% = \frac{A_0 - A}{A_0} \times 100$$

where $c$ is the concentration of the MB solution at the time $t$, $c_0$ is the equilibrium concentration of MB, and $A$, $A_0$ is the corresponding values achieved by measuring the absorbance at 665 nm with UV–Vis spectrometry. The mechanistic action of the catalytic oxidative dye degradation could be revealed when the following factors are monitored:

(a) Variation of pH

The influence of pH from 2 to 10 upon the degradation efficiency of MB dye was studied over catalyst dosage of 1 g/l at 40 °C under time intervals in between 0 and 8 hours, where initial MB and $H_2O_2$ concentrations are adjusted to $1 \times 10^{-4}$ M and 28.91 mM, respectively.

(b) Variation of MB dye concentration

Different concentrations ($3.24 \times 10^{-4}$, $1.00 \times 10^{-4}$ and $1.00 \times 10^{-5}$ M) of MB dye were prepared to investigate the effect of dye concentration on the extent of degradation over catalyst dosage of 1 g/l at 40 °C and pH 8.0 for 8 h.

(c) Variation of contact time

The kinetics of degradation process of MB dye were followed up at different contact times, applying both pseudo first-order and second-order models for the rate expressions, as:

$$k_1 t = Ln(C_0/C)$$

$$1/C = k + 2t + 1/C_0$$

where $k_1$ and $k_2$ represent the pseudo first-order rate constant ($h^{-1}$) and the pseudo second-order rate constant (L $mg^{-1}$ $h^{-1}$), respectively. In a typical kinetic experiment, 50 ml of a known concentration of the dye methylene blue solution were mixed with a known concentration of $H_2O_2$ at pH 8. This mixture is thermostated at 40 °C. The reaction started by adding 0.05 g of the supported catalyst. The progress of the reaction was followed by monitoring the decrease in the absorbance of methylene blue at 665 nm using UV–vis spectrophotometer.

## 3. Results and discussion

### 3.1. XRD analysis

#### 3.1.1. XRD of the raw and modified montmorillonite clays

The XRD patterns of parent montmorillonite clay and modified clays are illustrated in Fig. 1. The parent montmorillonite clay shows a basal (001) and (002) reflections at $2\theta = 6.95°$ and 12.4° with d-spacing 1.26 nm and 0.705 nm, respectively, [32,33]. The diffractions of $2\theta$ of around 19.8° was the summation of hk indices of (02) and (11) arises from the diffraction of random stacking of layers. The peak at $2\theta$ of 21.2° indicates also the reflection of (101) plane of OCT (opal-CT as Para crystalline silica, $SiO_2 \cdot H_2O$). Accessory minerals such as quartz were detected in clay sample at $2\theta$ of 26.78°.

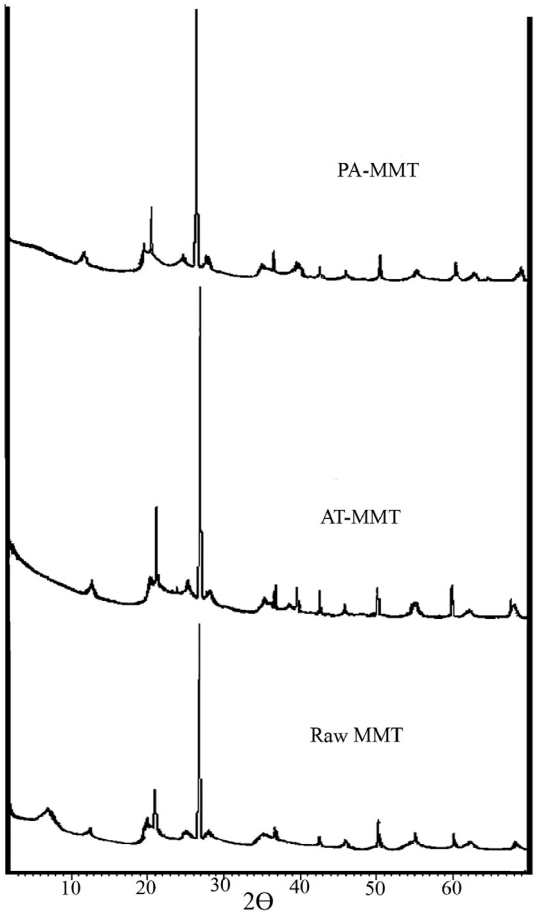


**Figure 1** XRD pattern of Raw and modified montmorillonite clay samples.

As a notice the considerably, the low value of the full width at half maximum peak height (FWHM) characteristic for *d* (001) basal peak points to the high stacking order of TOT elementary layers in the clay [34].

For the acid activated montmorillonite sample (AT-MMT) important mineralogical changes were induced and are seen from XRD patterns. The most pronounced modification noticed is the significant increment in the d-spacing of interlayered sheet structure of montmorillonite clay from 6.95° to 12.03° corresponding to (002) reflection. Also, the basal (001) reflection vanished indicating marked changes in the ordering of stacked interlayers. The OCT- characteristic peak is highly intensified pointing to a marked distortion of the layered structure of clay.

Upon treating clay with ρ-amino benzoic acid, the basal (001) reflection disappeared while (002) one was intact. This may reflect the availability of organic compound to have been driven into interlamellar sheet structure of montmorillonite clay resulting in the expansion of interlayered space and as reported by Jagtap [35]. The intercalation of ρ-ABA led to a decrease in the intensities of (02) and (11) diffraction peaks.

### *3.1.2. XRD study of the modified clay-immobilized copper nanoparticles*

XRD patterns of Cu immobilized onto tow modified clay samples are shown in Fig. 2.

For copper immobilized various modified clays, no peaks characteristic for Cu particles appeared reflecting the existence of highly amorphous copper nanoparticles [36].

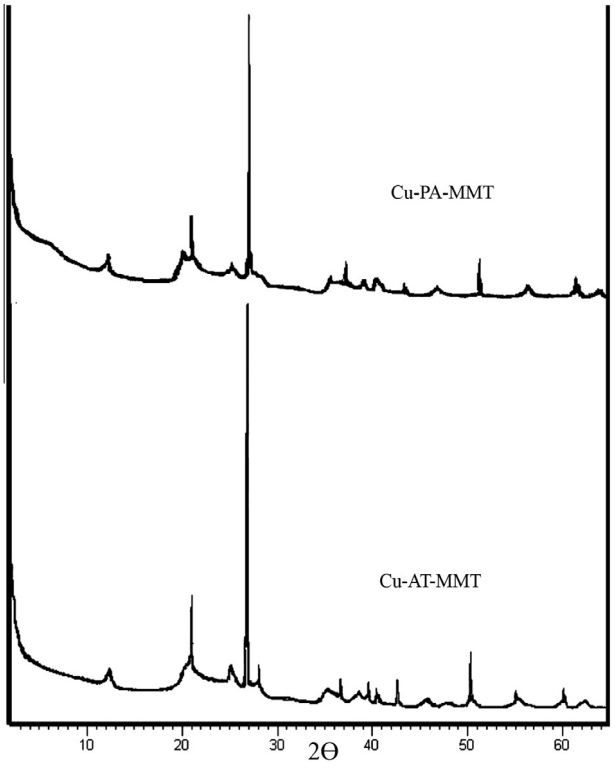


**Figure 2** XRD pattern of modified clays immobilized copper nanoparticles.

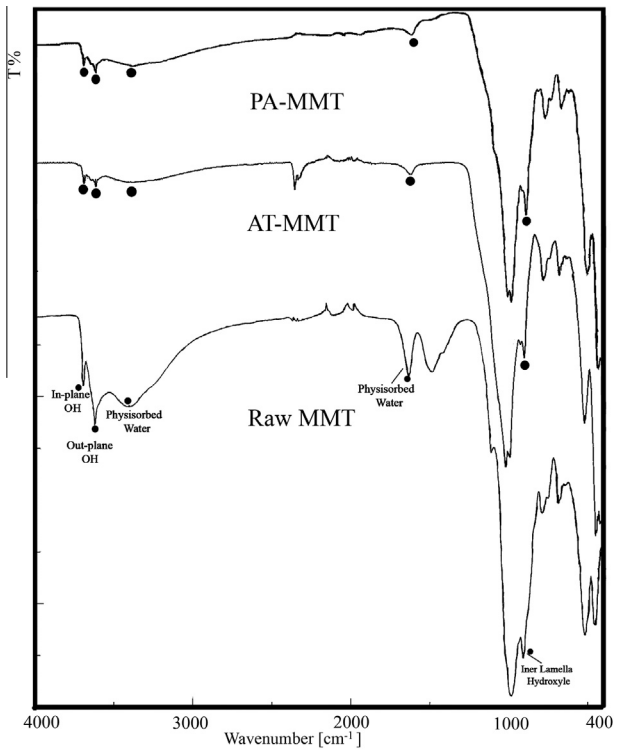


**Figure 3** FTIR bands of Raw and modified montmorillonite clay samples.

### *3.2. FT-IR spectroscopic structural analysis*

### *3.2.1. FTIR study of the raw and modified montmorillonite clays*

The FTIR bands of raw and modified clay samples are represented in Fig. 3. The original montmorillonite (Raw-MMT) exhibits broad bands at 3403 $cm^{-1}$ and 1633 $cm^{-1}$ reflecting

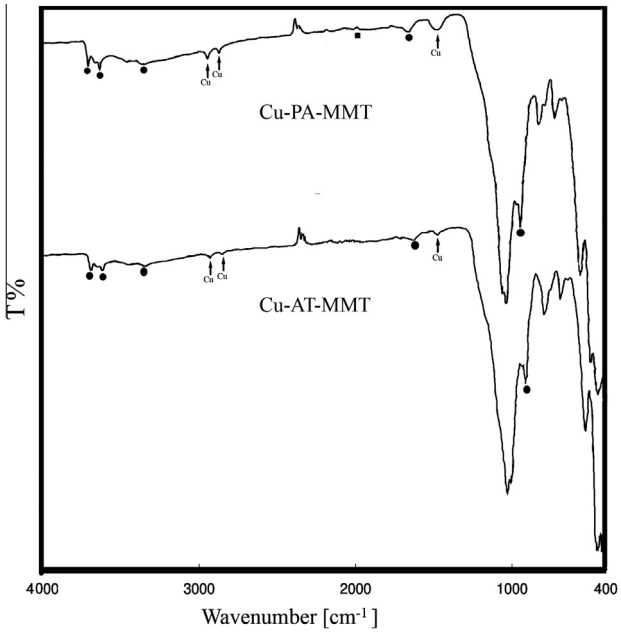


**Figure 4** FTIR bands of modified clays immobilized copper nanoparticles.

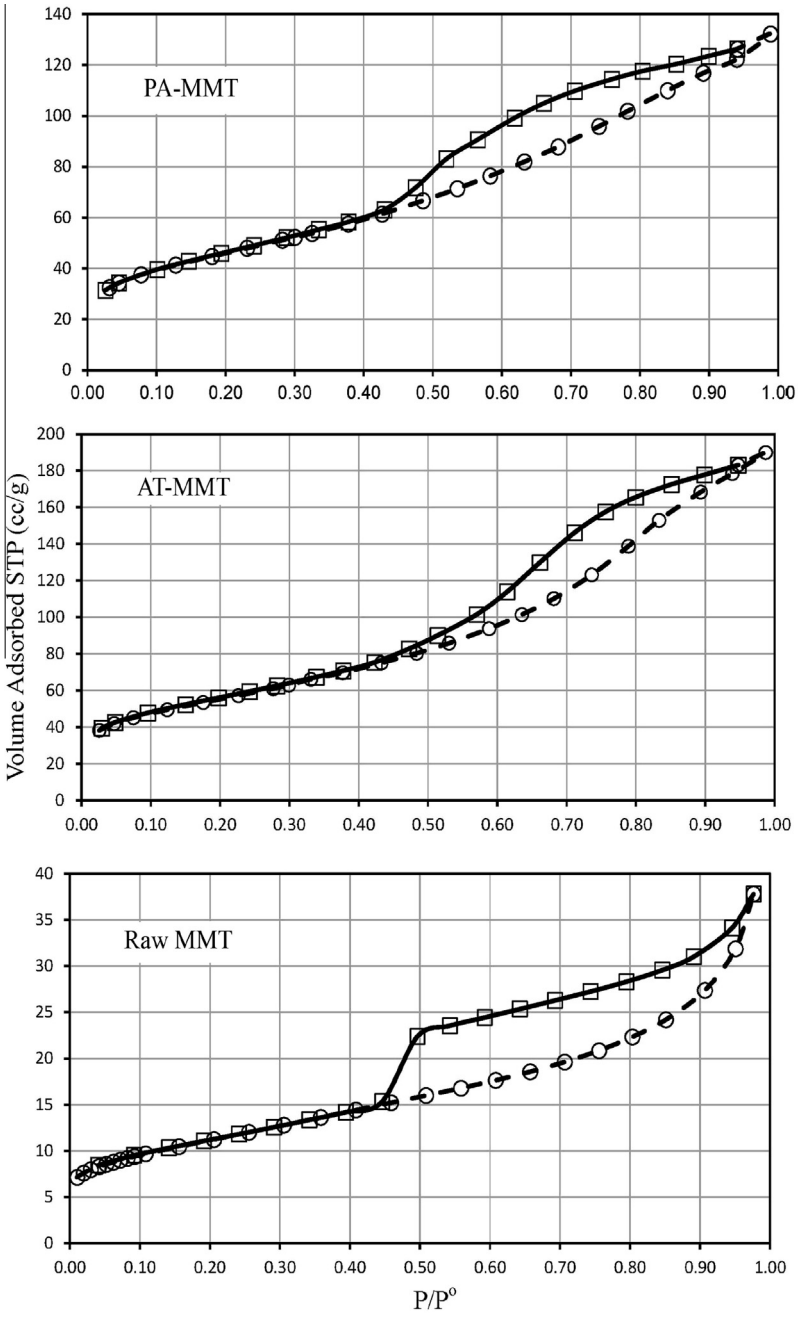


**Figure 5** Nitrogen adsorption–desorption isotherms of Raw and modified montmorillonite clay samples.

the stretched and bended vibrations of the water molecules present in the montmorillonite, respectively, [37]. The band at 3618 $cm^{-1}$ with a shoulder at about 3693 $cm^{-1}$ indicates the vibrations of hydroxyl groups bonded to octahedral cation (Al, Mg and Fe) [38]. The band at 908 $cm^{-1}$ confirms the dominant presence of dioctahedral smectite with [AlAl-OH] bending bands, band ranges between 460 and 1112 $cm^{-1}$ correspond to the phyllosilicate structure, which is associated with stretching and angular deformations of Si–O–Si and Si–O–Al [39].

In acid activated montmorillonite (AT-MMT) sample the band at 1634 $cm^{-1}$ relative to the adsorbed water molecules hardly appeared associated with complete dehydroxylation of in-plane and out-plane hydroxyl groups. Similar bands were observed in organically modified clay (PA-MMT) sample, in addition no peaks referring to the interaction between clay and organic molecules appeared confirming intercalation of ρ-ABA via columbic forces only.

### *3.2.2. FTIR spectra of the modified clay-immobilized copper nanoparticles*

The FTIR bands of copper immobilized onto various modified clay solid fractions are represented in Fig. 4.

For both types of the modified clay immobilized copper nanoparticles samples, bands around 2928, 2855 and 1476 $cm^{-1}$ appeared confirming the immobilization of copper

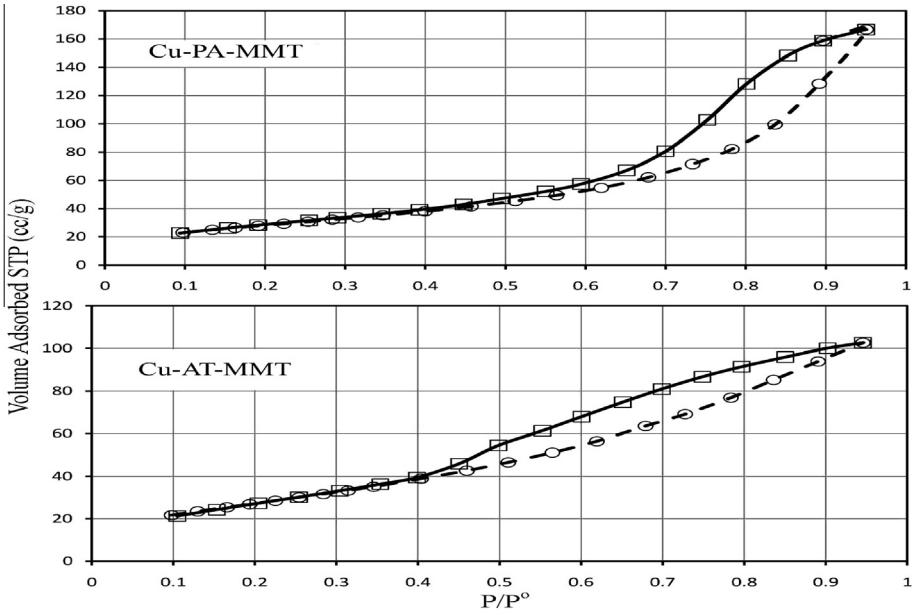


**Figure 6** Nitrogen adsorption–desorption isotherms of modified clays immobilized copper nanoparticles.

**Table 1** Structural and textural parameters of different samples under investigation.

| Catalyst samples | $C_{BET}$[a] | $S_{BET}$[a] ($m^2\ g^{-1}$) | Total pore volume[b] (mL $g^{-1}$) | Average pore radius[b] (Å) |
|---|---|---|---|---|
| Raw-MMT | 243.08 | 39.17 | 0.058 | 29.97 |
| AT-MMT | 178.89 | 195.07 | 0.295 | 30.24 |
| PA-MMT | 177.17 | 162.22 | 0.205 | 25.03 |
| Cu-AT-MMT | 63.50 | 104.12 | 0.258 | 49.56 |
| Cu-PA-MMT | 48.02 | 103.29 | 0.159 | 30.74 |

[a] Calculated from nitrogen adsorption isotherm using the BET equation.
[b] Determined from nitrogen adsorption isotherm.

nanoparticles in clay matrices through conformational changes in metal linked clay interactions [40,41]. The structure of the two different modified clay samples were unaffected by copper embedment into clay galleries.

Moreover, a new peak appeared in spectrum of Cu-PA-MMT sample at 1955 $cm^{-1}$ relative to $-NH_2$ stretching frequencies inferring involvement of weak H-bonding between ρ-ABA molecule and interlamellar hydroxyls of the clay mineral.

### 3.3. Morphological properties

#### 3.3.1. Texture properties of modified montmorillonite samples, and Cu supported modified clay nanocomposites

The adsorption-desorption isotherms of $N_2$ at −196 °C of various modified clay samples and various metal/clay nanocomposites are shown in Figs. 5 and 6.

The shape of all adsorption isotherms is characteristic for Type II behavior according to IUPAC with hysteresis loop of type H3. This shape of hysteresis characterizes mainly mesoporous solids, often associated with uniform aggregates of plate-like particles giving rise to slit-like pores, exhibiting some microporosity [42–44].

It can be seen from Table 1 that, the raw montmorillonite (Raw-MMT) has a high energetic surface of a low surface area and predominance of narrow fractions of mesopores. In contrast, the acid treated (AT-MMT) sample displays a marked increase in surface area and total pore volume. These findings most probably reflect the great extent of deterioration in the stacking manner of clay layered sheet orientation, where the middle part of pores are largely expanded resulting in the elevation of pore volume as well surface area. For organically modified clay, the increment in surface area and total pore volume with a slight decrease in the average pore radius revealed intercalation of organic compound into the TOT interlamellar spaces.

Immobilizing Cu-metallic nanoparticles over acid treated clay reduces the surface potential and cause dramatic falling in surface area and total pore volume with a significant increase in the average pore radius, this increase may be due to the rupture of some smaller pores to generate bigger ones

during the immobilization of Cu-nanoparticles into the pores [11]. For organically modified immobilized metal nanoparticles, the poor surface parameter values indicate the location of metallic particles near to edges resulting in blockage of interlayers.

*3.3.2. Cation exchange capacity of various modified montmorillonite samples*

The raw montmorillonite exhibits a quite large CEC of 50 meq/100 g characterizing generally the (TOT) structures [45]. By acid treatment of clay, the CEC decreased to

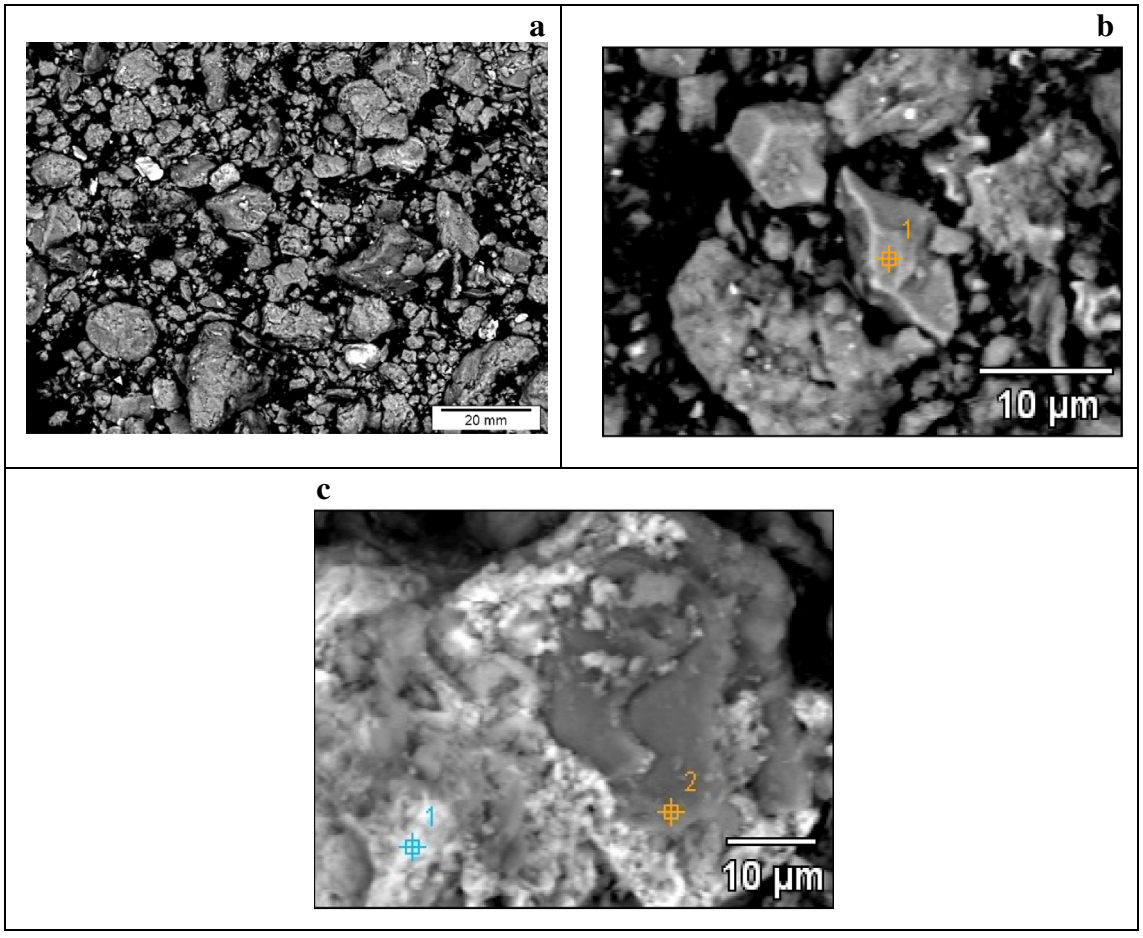


**Figure 7** SEM images of (a) Raw montmorillonite clay, (b) acid-treated, (c) organo-treated montmorillonite clay.

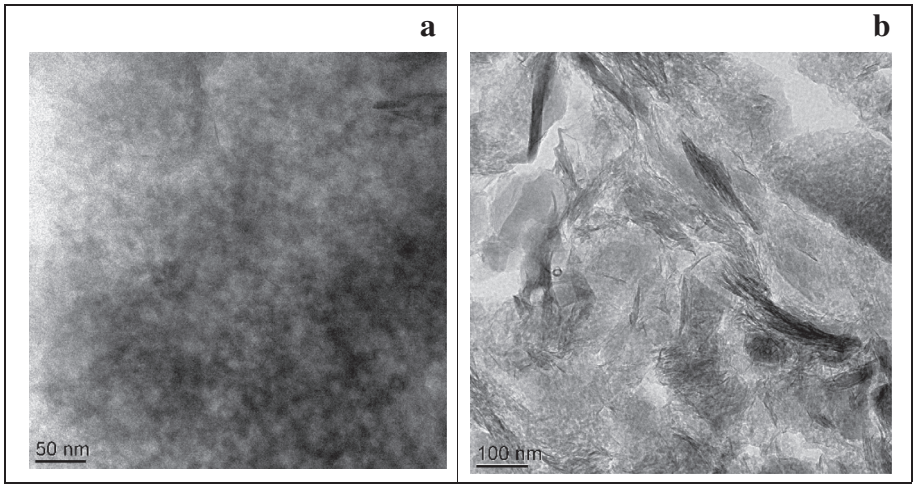


**Figure 8** TEM images of copper nanoparticles immobilized onto (a) acid treated, (b) organo-treated montmorillonite clay.

24 meq/100 g replacing foreign exchangeable cations by $H^+$ from sulfuric acids, [46]. Upon chemical modification of montmorillonite with ρ-ABA the CEC decreases achieving 35 meq/100 g pointing to the loss of exchangeable atoms, as the large cationic ρ-ABA molecules mask some of the exchangeable cations in the interlayer space [47].

### 3.3.3. Scanning electron microscopy of various modified montmorillonite samples

The scanning electron microscope micrographs of parent and various modified clay samples are illustrated in Fig. 7. The parent montmorillonite clay owed compact layered TOT sheet structure being organized in aggregated patches of uneven particle sizes. With acid activation, the large interlayered clay aggregates were cracked to smaller uneven flakes of semi-flat surfaces (Fig. 7b) [48]. In other words, the SEM image of acid treated montmorillonite confirmed that clay lamellar structure was damaged by acid treatment, as being evidenced elsewhere [49]. The micrograph of organically modified clay reveals the existence of highly ordered lamellar sheet structure, which most probably originated from the intercalation of heavy organo-materials.

### 3.3.4. Transmission electron microscopy of Cu nanoparticles modified clay nanocomposites

The particle size and morphology of the as prepared copper nanoparticles were examined by transmission electron microscopy (TEM) as being depictured in Fig. 8.

The metallic Cu particles immobilized onto acid treated clay are spherical in shape with a minute particle size achieving 8 nm and highly dispersed over clay sheets. Also, the interlamellar sheet structure of montmorillonite clay seems to be highly destructed. Immobilization of Cu-particles within organo-treated clay developed intercalation regions with little zones of exfoliation, where the layered sheet structure was disoriented and suffers a lot of fracturing and aggregates of Cu species were observed with extended needle-like shape of length approximately 120 nm.

## 3.4. Oxidative catalytic degradation of methylene blue dye by various modified clay immobilized metallic nanoparticles

### 3.4.1. Effect of pH

The reaction pH value is one of the most important parameters that affect the decoloration process of dyes. pH values of MB dye solution ranging from 2 to 10 were investigated as shown in Fig. 9.

The results indicate that the degradation rates increase by increasing the reaction pH values. For the two copper/clay nanocomposites the weak alkaline medium (pH = 8) adopted relatively better degradation efficiencies than those of the neutral and acidic mediums. Such behavior seems to be attributed to the fact that $H_2O_2$ deprotonation is accelerated in elevated pH values, where the decomposition rate of is highly augmented [50]. On the other hand, although MB is a cationic dye in aqueous solution, existence of both MB dye and catalyst in an acidic pH enforced them to attain positive charges,

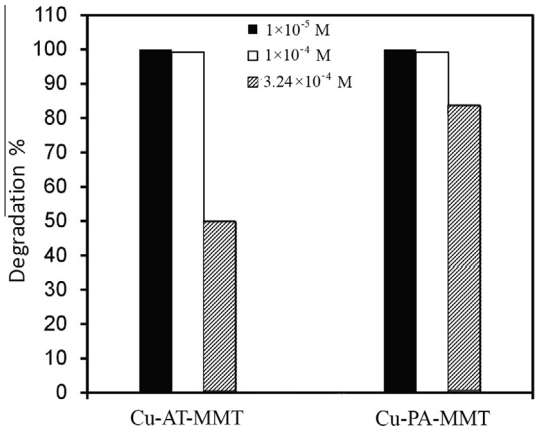


**Figure 10** Effect of initial MB dye concentration on degradation efficiency of MB. conditions: $[H_2O_2]_0$ = 28.91 mM; pH = 8.0; catalyst dosage = 1.0 g $L^{-1}$; time = 8 h, $T$ = 40 °C.

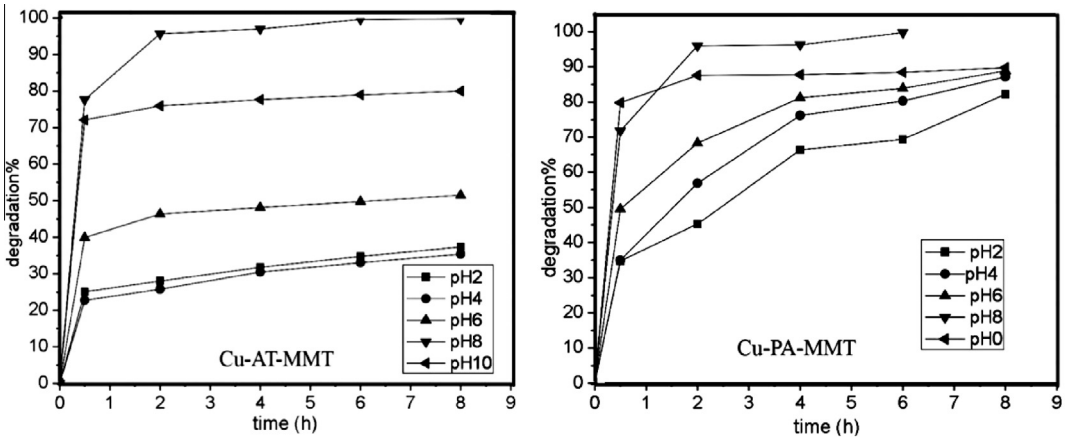


**Figure 9** The effect of initial pH values on degradation of MB over modified clays immobilized copper nanoparticles. conditions: $[H_2O_2]_0$ = 28.91 mM; $[MB]_0$ = 1 × $10^{-4}$ M; catalyst dosage = 1.0 g $L^{-1}$; time = 8 h, $T$ = 40 °C.

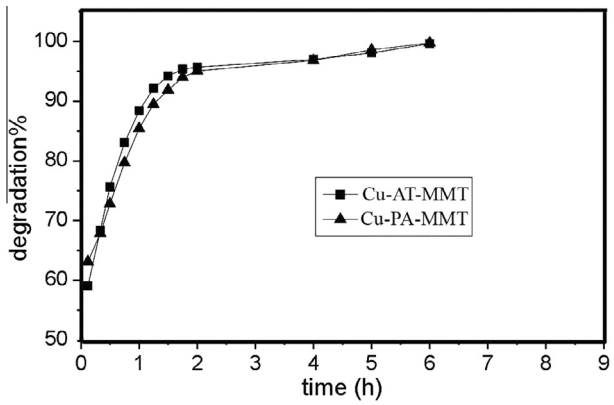


**Figure 11** Degradation kinetics of MB dye over modified clays immobilized copper nanoparticles. Conditions: $[H_2O_2]_0 = 28.91$ mM; $[MB]_0 = 1 \times 10^{-4}$ M; pH = 8.0; catalyst dosage = 1.0 g $L^{-1}$; $T = 40$ °C.

which, in turn, arise as a strong electrostatic repulsion between them retarding the degradation capability of MB dye. While in basic medium, MB accepts cationic character and the catalyst attains a negative charge. Thus, there would be electrostatic attraction enhancement.

It is worth mentioning that the degradation process over organo-modified immobilized Cu NPs showed elevated degradation efficiencies achieving 100%. This phenomenon could be due to the availability of organo-treated montmorillonite clay to adopt suitable media for Cu nanoparticles in order to acquire an inexhaustible redox reaction, where reactant molecules are allowed to move freely over oxidative catalytic centers (Cu NPs). Such suggestion is highly evidenced by surface characterization and TEM studies.

### 3.4.2. Effect of dye concentration

Many researchers investigated the effect of initial concentration on the degradation of dyes in solution [51,52], The effect of initial dye concentration on the degradation efficiency is shown in Fig. 10. It can be seen that the degradation efficiency of methylene blue is inversely proportional to its concentration, which means, the lower of the dye concentration, the higher the efficiency of the dye degradation as the degradation efficiency relates to the formation of hydroxyl radicals, increasing initial concentration of MB dye in solution lead to adsorption of high extents of heavy MB organic compounds rendering interactions between the metallic catalytic sites and the oxidant molecules ($H_2O_2$). Thus, the amount of generated oxidizing species could suffer marked leakage causing a great reduction in the degradation efficiency of MB dye [53].

### 3.4.3. Effect of contact time

Kinetics study is important for any catalytic reaction and helps in identifying the reaction pathways as well the rate dependence on the limiting reacting system. In this respect, degradation activities of metal/clay nanocomposites are represented in Fig. 11.

It is noted that copper immobilized onto acid as well as organo-treated clay exhibits complete decomposition of the MB dye molecules within 2 h.

The kinetic plots of oxidative MB degradation over various metal/clay nanocomposites are illustrated in Fig. 12 in addition to the degradation kinetic and equilibrium data which are detailed in Table 2.

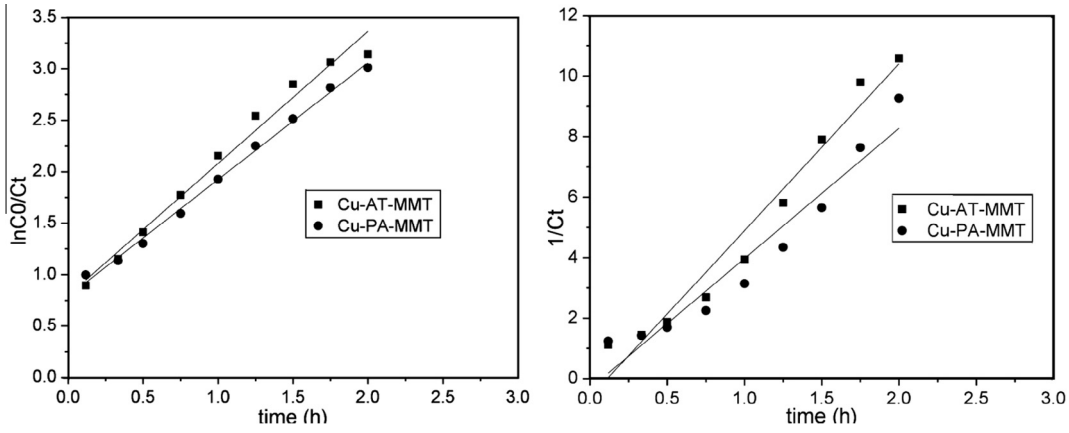


**Figure 12** First order and second order plots for MB degradation onto modified clays immobilized copper nanoparticles.

**Table 2** Degradation kinetic and equilibrium data, corresponding to oxidative MB degradation using copper nanoparticles embedded tow modified clays under reaction conditions of $[H_2O_2]_0 = 28.91$ mM; $[MB]_0 = 1 \times 10^{-4}$ M; catalyst dosage = 1.0 g $L^{-1}$; pH 8.0; time 2.0 h; and temperature 40 °C.

| Catalyst type | % MB degradation at equilibrium | First order | | Second order | |
|---|---|---|---|---|---|
| | | $k_1$ ($h^{-1}$) | $R^2$ | $k_2$ (L $mg^{-1}$ $h^{-1}$) | $R^2$ |
| Cu-AT-MMT | 95.6 | 1.284 | 0.982 | 5.512 | 0.96 |
| Cu-PA-MMT | 95 | 1.143 | 0.995 | 4.302 | 0.927 |

It is likely that copper/clay nanocomposite perpetuates first ordered oxidative degradation process, where the low molecular weight oxidant ($H_2O_2$) becomes the only possible adsorbate over metallic sites. Such oxidant was catalytically decomposed throwing out plenty of powerful oxidizing oxygen radicals toward the solution, in which methylene blue molecules eagerly interact with those radicals initiating the decay of MB into smaller fragments, as being illustrated in Scheme.

Initiation step

$$M^0 + H_2O_{2(aq)} = M^{+n} + HO^-_{(aq)} + HO^{\cdot}_{(aq)}$$

Propagation steps

$$HO^{\cdot}_{(aq)} + H_2O_{2(aq)} = HO^{\cdot}_{2(aq)} + H_2O_{(liq)}$$

$$HO^{\cdot}_{(aq)} + MB \rightarrow H_2O_{(liq)} + MB^{\cdot}$$

$$HO^{\cdot}_{2(aq)} + MB \rightarrow H_2O_{2(aq)} + MB^{\cdot}$$

$$MB^{\cdot} \rightarrow \text{further oxidation}$$

Termination steps

$$HO^{\cdot}_{2(aq)} + M^{+n} = M^0 + H^+_{(aq)} + O_{2(g)} (\text{regeneration step})$$

$$HO^{\cdot}_{2(aq)} + HO^{\cdot}_{2(aq)} = H_2O_{2(aq)} + O_{2(g)}$$

$$HO^{\cdot}_{2(aq)} + HO^{\cdot}_{(aq)} = H_2O_{2(aq)} + O_{2(g)}$$

## 4. Conclusion

Copper nanoparticles were prepared using reduction methods and then supported onto acid and organo treated montmorillonite clay. The Cu supported clay were then used as catalyst for methylene blue dye degradation. The results confirmed that copper/clay nanocomposite can be used to efficiently degrade MB dye especially at an increased pH of 8 which expressed the best degradation efficiencies. The degradation efficiency seems to be sensitive to the initial concentration of MB dye where a critical concentration is defined. While Cu supported organo treated clay showed a higher degradation efficiency that reaches 100%. Future efforts of similar metallic supports are needed to allow accommodating higher concentration of various organic dyes water pollutants treatment with the focus on type and concentration.

## References


[1] D.L. Feldheim, C.A. Foss Metal, Nanoparticles, Synthesis, Characterization, and Applications, Marcel Dekker AG, Switzerland, 2002.
[2] W. Xie, Y. Li, Z.Q. Liu, M. Haruta, W.J. Shen, Nature 458 (2009) 746–749.
[3] E. Formo, E. Lee, D. Campbell, Y. Xia, Nano Lett. 8 (2008) 668–672.
[4] N. Zheng, G.D. Stucky, J. Am. Chem. Soc. 128 (2006) 14278–14280.
[5] A.A. Ponce, K.J. Klabunde, J. Mol. Catal. A. 225 (2005) 1–6.
[6] Z. Huang, F. Cui, H. Kang, J. Chen, X. Zhang, C. Xia, Chem. Mater. 20 (2008) 5090–5099.
[7] J.M. Campelo, T.D. Conesa, M.J. Gracia, M.J. Jurado, R. Luque, J.M. Marinas, A.A. Romero, Green Chem. 10 (2008) 853–858.
[8] S. Pande, A. Saha, S. Jana, S. Sarkar, M. Basu, M. Pradhan, A. K. Sinha, S. Saha, A. Pal, T. Pal, Org. Lett. 10 (2008) 5179–5181.
[9] S.W. Kim, M. Kim, W.Y. Lee, T. Hyeon, J. Am. Chem. Soc. 124 (2002) 7642–7643.
[10] O.S. Ahmed, D.K. Dutta, Thermochim. Acta 395 (2003) 209–216.
[11] D. Dutta, B.J. Borah, L. Saikia, M.G. Pathak, P. Sengupta, D. K. Dutta, Appl. Clay Sci. 53 (2011) 650–656.
[12] P. Sharma, S.K. Bhorodwaj, D.K. Dutta, J. Sci. Conf. Proc. 1 (2009) 40–43.
[13] M. Tamura, H. Fujihara, J. Am. Chem. Soc. 125 (2003) 15742–15743.
[14] V.K. Sharma, R.A. Yngard, Y. Lin, Adv. Colloid Interface Sci. 145 (2009) 83–96.
[15] N. Mahata, A.F. Cunha, J.J.M. Orfao, J.L. Figueiredo, Catal. Commun. 10 (2009) 1203–1206.
[16] O.S. Ahmed, D.K. Dutta, Langmuir 19 (2003) 5540–5541.
[17] P.P. Sarmah, D.K. Dutta, Green Chem. 14 (2012) 1086–1093.
[18] B.J. Borah, D. Dutta, P.P. Saikia, N.C. Barua, D.K. Dutta, Green Chem. 13 (2011) 3453–3460.
[19] H. Patel, A. Hasmukh, H.C. Bajaj, R.V. Jasra, J. Nanopart. Res. 10 (2008) 625–632.
[20] B.J. Borah, D. Dutta, D.K. Dutta, Appl. Clay Sci. 49 (2010) 317–323.
[21] S. Zulfiqar, A. Kausar, M. Rizwan, M.I. Sarwar, Appl. Surf. Sci. 255 (2008) 2080–2086.
[22] N.R. Shiju, V.V. Guliants, Appl. Catal. A: Gen. 356 (2009) 1–17.
[23] F. Thibault-Starzyk, M. Daturi, P. Bazin, O. Marie, in: D. Astruc (Ed.), Nanoparticles and Catalysis, Wiley-VCH, New York, 2008, pp. 505–528.
[24] V. Polshettiwar, R.S. Varma, Green Chem. 12 (2010) 743–754.
[25] Y. Xi, M. Megharaj, R. Naidu, Appl. Clay Sci. 53 (2011) 716–722.
[26] Z. Chen, T. Wang, X. Jin, Z. Chen, M. Megharaj, R. Naidu, in: J. Colloid Interf. Sci. 398 (2013) 59–66.
[27] Y. Yang, J. Luan, Molecules 17 (2012) 2752–2772.
[28] R.S. Mikhail, S. Brunauer, E.E. Boder, J. Colloid Interface Sci. 26 (1968) 45–53.
[29] S. Brunauer, P.H. Emmett, E. Teller, J. Am. Chem. Soc. 60 (1938) 308–319.
[30] L. Ammann, Cation exchange and adsorption on clays and clay minerals. Thesis, University of Kiel, Germany, 2003.
[31] L. Ammann, F. Bergaya, G. Lagaly, Clay Miner. 40 (2005) 441–453.
[32] R.T. Yang, N. Tharappiwattananon, R.Q. Long, Appl. Catal. B 19 (1998) 289–304.
[33] M. Yurdakoç, M. Akcay, Y. Tonbul, F. Ok, K. Yurdakoç, Microporous Mesoporous Mater. 111 (2008) 211–218.
[34] M. Lenarda, L. Storato, G. Pellegrini, L. Piovesan, R. Grnzerla, in: Mol. Catal. A: Chem. 145 (1999) 237–244.
[35] N. Jagtap, V. Ramaswamy, Appl. Clay Sci. 33 (2006) 89–98.
[36] C. Dong, H. Cai, X. Zhang, C. Cao, Physica E Low dimens Syst Nanostruct. 57 (2014) 12–20.
[37] V. Sontevska, G. Jovanovski, P. Makreski, J. Mol. Struct. 834–836 (2007) 318–327.
[38] J. Madejová, Vib. Spectrosc. 31 (2003) 1–10.
[39] C. Bertagnolli, S.J. Kleinübing, M.G.C. da Silva, Appl. Clay Sci. 53 (2011) 73–79.
[40] R. Das, S.S. Nath, R. Bhattacharjee, J. Fluoresc. 21 (2011) 1165–1170.
[41] B. Bagchi, S. Kar, S.K. Dey, S. Bhandary, D. Roy, T.K. Mukhopadhyay, S. Das, P. Nandy, Colloid Surf. B Biointerface 108 (2013) 358–365.
[42] H. Noyan, M. Onal, Y. Sarikaya, Food Chem. 105 (2007) 156–163.

[43] J.P. Nguetnkam, R. Kamga, F. Villieras, G.E. Ekodeck, A. Razafitianamaharavo, J. Yvon, J. Colloid Interf. Sci. 289 (2005) 104–115.
[44] L. Chmielarz, P. Kustrowski, M. Zbroja, A.R. Lasocha, B. Dudek, R. Dziembaj, Appl. Catal. B. 45 (2003) 103–116.
[45] F. Ayari, E. Srasra, M. Trabelsi-Ayadi, Desalination 185 (2005) 391–397.
[46] J. Wakim, Influence des solutions aqueuses sur le comportement mécanique des roches argileuses, France, Thèse de doctorat, Ecole nationale supérieure des mines de Paris, 2005.
[47] K.G. Bhattacharyya, S.S. Gupta, Colloids Surf. A 277 (2006) 191–200.
[48] M. Auta, B.H. Hameed, Chemistry 19 (2013) 1153–1161.
[49] O.B. Ayodele, B.H. Hameed, Appl. Clay Sci. 83–84 (2013) 171–181.
[50] I.A. Salem, Appl. Catal. B 28 (2000) 153–162.
[51] H.Y. Shu, M.C. Chang, J. Hazard. Mater. 125 (2005) 96–101.
[52] H.Y. Shu, M.C. Chang, H.J. Fan, J. Hazard. Mater. 113 (2004) 201–208.
[53] R.M. Mohamed, E.S. Baeissa, I.A. Mkhalid, M.A. Al-Rayyani, Appl. Nanosci. 3 (2013) 57–63.